Materials Advances

ROYAL SOCIETY OF CHEMISTRY

PAPER

View Article Online
View Journal | View Issue



Cite this: *Mater. Adv.*, 2026, 7, 447

# Enhancing short-term electron exchange in pyrogenic carbonaceous materials through post-pyrolysis oxidative treatments

Ethan Quinn, Detlef R. U. Knappe and Douglas F. Call *

Pyrogenic carbonaceous materials (PCMs) can mediate environmentally beneficial redox reactions through electron exchange with contaminants and microorganisms. Electron exchange kinetics and capacities of PCMs are generally too low for applications that operate on short time scales, such as contaminant pump and treat reactors and biological activated carbon systems. Here, we aimed to increase electron exchange kinetics and capacities over the short term (hours) using a high-surface area activated carbon cloth (ACC) derived from a highly pure novoloid phenol-aldehyde feedstock subjected to oxidative treatments [hydrogen peroxide ($H_2O_2$) and nitric acid ($HNO_3$)]. Mediated electrochemical reduction experiments revealed substantial increases in both the magnitude and rate of electron accepting capacity (EAC) resulting from oxidative treatment. $HNO_3$-treated ACC reached a maximum EAC of 9.16 ± 0.36 mmols $e^-$ per g-AC (30 min $HNO_3$ treatment) within 5–6 hours, a 5.1× increase relative to the non-treated ACC. The initial electron transfer rate (within the first 30 min) of the $HNO_3$-treated ACC reached a maximum of 0.11 ± 0.02 mmols $e^-$ per g-AC per min, which was ~3.5× faster than the non-treated ACC. We observed both an increase in oxygen content throughout the ACC and decrease of micropore volume after $HNO_3$ treatment, suggesting that electron exchange kinetics were improved by the appearance of additional redox-active oxygen groups and improved transport of the electron mediator in and out of the ACC pores. $H_2O_2$ treatment increased only the exterior surface oxygen content and was associated with loss of some redox functionality over time. These findings further our understanding of the physicochemical properties that contribute to PCM electron transfer and help transition reactive PCMs toward applications that would benefit from rapid redox transformations.

Received 8th July 2025,
Accepted 12th November 2025

DOI: 10.1039/d5ma00727e

rsc.li/materials-advances



## 1. Introduction

The adsorptive and reactive properties of pyrogenic carbonaceous materials [PCMs; *e.g.*, activated carbon (AC), biochar] offer unique opportunities to mediate chemical and biological transformations in engineered and natural environments. PCMs can have a large adsorptive capacity for many contaminants, especially organic contaminants.[1,2] They can also transfer electrons to some contaminants through abiotic and biotic reduction reactions that can yield less harmful transformation products.[3–7] PCMs can also mediate electron transfer between microorganisms.[8] Linkages between PCM physical and chemical properties and electron exchange capabilities have been established, but less progress has been made on "fine tuning" those properties to broaden applications, especially in engineered systems.

Currently, the timescales over which PCMs exchange electrons are long, relative to those of engineered systems that operate over short timescales.[9] For *in situ* remediation of natural environments, such as contaminated sediments, longer timescales (*e.g.*, months) of contaminant removal typically occur. Slower PCM electron exchange is therefore suitable. However, in applications such as pump and treat treatment reactors, drinking water treatment (*e.g.*, biological activated carbon), and wastewater treatment, reactor retention times range from a few minutes to hours.[10–12] In those situations, fast electron transfer to/from contaminants/microbes is important. Most PCMs studied to date exhibit electron transfer rates that are too slow to provide meaningful reactivity in these types of applications.

Electron transfer in PCMs is driven by both material conductivity and redox-active functionalities. Deficiency in one or both properties can have a significant impact on material redox performance. Across all PCMs, biochars typically exhibit the lowest electrical conductivity, sometimes by an order

*Department of Civil, Construction, and Environmental Engineering, North Carolina State University, Campus Box 7908, Raleigh, USA. E-mail: dfcall@ncsu.edu*

of magnitude.[13,14] Though some biochars have been found to have a substantial electron exchange capacity (EEC), the kinetics of electron transfer are often hindered by singular reliance on reactive functional groups.[3] AC generally has a higher degree of graphitization, leading to higher conductivity, as well as a much higher surface area. While this increase in surface area can provide more reactive sites for EECs, electron transfer kinetics can be hindered by the highly microporous nature of the materials limiting access to reactive sites.[4,9,15,16] PCM enhancement, either during synthesis or through post-synthesis modifications, to generate favorable conductive capabilities and accessible redox-active functionalities may enable faster reaction times.

In addition to rate, short-retention treatment systems would benefit from improvements in the total amount of electrons exchanged over short timescales. If there are limited electrons either stored in the PCMs or that can react with contaminants *via* redox-active functional groups, then thorough transformations of contaminants, especially those requiring high numbers of electrons (*e.g.*, $NO_3^-$ reduction to $N_2$ gas, nitrobenzene reduction to aniline) or that are present in high concentrations, may be limited.[17,18] Current EECs are often reported in the range of 0.1–1 mmols $e^-$ per g-PCM, and vary widely depending on material and analysis type.[4,15,19,20] Most evidence points to quinone and phenolic groups as the primary contributors to EEC.[15,21] Quinones are suspected of electron acceptance and donation, whereas phenols are believed to participate only in electron donation. There are a variety of strategies to promote formation of these groups on PCMs, including oxidative treatments with chemicals such as hydrogen peroxide and nitric acid. A challenge for gaining clear mechanistic insight when synthesizing PCMs or modifying them post-synthesis, is that multiple properties (physical and chemical) can change simultaneously.

Here we aimed to develop PCMs with faster electron exchange and higher electron acceptance capacities over short time periods. Doing so would help inform the design of PCMs for contaminant and biological transformations in applications that require fast (minutes to hours) electron transfer and large numbers of electrons. To improve clarity on mechanisms underlying kinetic and capacity changes, we used an AC derived from a material (novoloid phenol-aldehyde fiber) that is highly pure relative to traditional PCM feedstocks (wood, straw, *etc.*). Additionally, we used a new form of PCM whose EEC has not been reported: a monolithic cloth that is highly porous, scalable, and applicable to flow-through processes relevant to many water treatment systems.[22] Using an electrochemical mediated method, we found that the AC cloth (ACC) accepted electrons at high rates and capacities. Oxidative chemical treatments that deposited putative electron accepting functional groups increased rates and capacities significantly, reaching some of the highest reported values to date. These findings further our understanding of the physicochemical properties of PCMs associated with EEC and help transition PCMs to applications that operate over short timescales.

# 2. Materials and methods

## 2.1 Activated carbon cloth treatments

Commercial ACC was purchased from Kynol (ACC-5092-15), cut into 1 × 1 cm pieces, and washed in 200 mL deionized (DI) water to remove dust and debris. Non-treated samples (X-AC), which represent controls, were oven-dried at 70 °C after the DI wash. Each treatment consisted of soaking 1 × 1 cm pieces (4–5 pieces per treatment) in the chemical oxidizers for a predetermined amount of time. $H_2O_2$ [9.8 M (30%); Fisher Scientific] treated samples ($H_2O_2$-AC) were soaked in 200 mL for 2 min, 5 min, 30 min, and 24 hours. $HNO_3$ (7.9 M; Fisher Scientific) treated samples ($HNO_3$-AC) were soaked in 200 mL for 30 s, 5 min, 30 min, and 24 hours. All incubations were performed in triplicate under constant mixing (250 rpm) at room temperature. After treatment, the samples were washed in 200 mL DI for ∼5 min, dried at 70 °C, and stored in covered aluminum weighing dishes at ambient conditions until use.

## 2.2 Electrochemical analysis

Electrochemical experiments were performed in a 100-mL glass bulk electrolysis cell (MF-1056, BASi Research Products) comprised of a vitreous carbon working electrode (WE), a coiled platinum auxiliary electrode contained within a fritted glass chamber, and an Ag/AgCl reference electrode (+200 mV *vs.* standard hydrogen electrode). Mediated electrochemical reduction and mediated electrochemical oxidation (MEO) tests were performed as described previously.[19,23] Phosphate buffer was first prepared using sodium phosphate monobasic monohydrate ($NaH_2PO_4{\cdot}H_2O$) (MFCD00149208; Sigma Aldrich) and sodium phosphate dibasic heptahydrate ($Na_2HPO_4{\cdot}7H_2O$) (MFCD00149180; Fisher Scientific) in DI water for a final concentration of 0.1 M phosphate. Sodium chloride was added to serve as an electrolyte. The electrochemical cell was filled with 72 mL of buffer (3 M NaCl, 0.1 M phosphate, pH 7) and equilibrated with the WE set to a potential of −0.40 V in MER and +0.61 V in MEO (*vs.* Ag/AgCl) under constant stirring (∼200 rpm) with a stir bar. Once current stabilized and remained constant at a low value (<50 μA), 3 mL of the 10 mM chemical electron mediator stock solutions [MER: diquat dibromide monohydrate (DQ), Sigma Aldrich; MEO: 2,2′-azino-bis(3-ethylbenzothiazoline-6-sulfonic acid) diammonium salt (98%) (ABTS), Fisher Scientific] was spiked into the cell to give a working concentration of 0.4 mM. A reductive or oxidative peak appeared after spiking with DQ or ABTS, respectively. Once the current returned to the initial baseline value, an ACC sample (∼0.02 g) was added to the solution, resulting in new reductive (during MER) or oxidative (during MEO) current peaks. Numerical integration of the area under the peaks yielded the electron accepting capacity (eqn (1)) or the electron donating capacity (EDC; eqn (2)).

$$\mathrm{EAC} = \frac{\int \frac{I_{\mathrm{red}}}{F} \mathrm{d}t}{m_{\mathrm{ACC}}} \quad (1)$$

$$\mathrm{EDC} = \frac{\int \frac{I_{ox}}{F} dt}{m_{ACC}} \quad (2)$$

where, $I_{red}$ (A) and $I_{ox}$ are the reductive and oxidative currents, respectively. $F$ is the Faraday constant (96 485 C $mol^{-1}$), and $m_{ACC}$ (g) is the mass of the ACC. All MER and MEO tests were conducted in triplicate in an anaerobic chamber (1.5–3%$H_2$, 97–98.5% $N_2$) at room temperature to mitigate electron transfer to $O_2$.

### 2.3 Chemical property characterization

Elemental and functional group changes resulting from chemical treatment were analyzed *via* X-ray photoelectron spectroscopy (XPS). XPS analysis was carried out using a SPECS™ system instrument equipped with a PHOIBOS 150 analyzer under a pressure of $\sim 3 \times 10^{-13}$ bar. The instrument contained both MgKα X-ray ($h\nu$ = 1253.6 eV) and AlKα X-ray ($h\nu$ = 1486.7 eV) sources. The surface composition of the ACC was characterized using the MgKα X-ray source operating at 10 kV and 30 mA (300 W). Survey scans for analysis of elements were recorded with a pass energy of 24 eV in a step of 0.5 eV. High resolution scans, for targeted analysis of individual survey scan peaks, were done with a pass energy of 20 eV in a 0.1 eV step. The CasaXPS computer software was used to deconvolute binding energies into chemical functional groups.[24] Binding energies were sourced from the National Institute of Standards and Technology (NIST).[25]

Elemental composition on the surface and within the materials was characterized using CHN(O)S analysis (Measurlabs; Helsinki, Finland). Samples were dried for three hours at 105 °C and then stored under a helium atmosphere to avoid moisture absorption prior to analysis. The samples were first subjected to a flash combustion process at 1000 °C under 25 kPa of $O_2$ in a pure oxygen environment.[26,27] C, H, N, and S present in the samples were transformed into their combustion products, fed through copper to remove excess oxygen, separated *via* gas chromatography, and measured using a thermal conductivity detector. Oxygen content was determined indirectly through pyrolysis at 1480 °C in a hydrogen–helium ($H_2$–He) gas mixture. Oxygen-containing species throughout the samples were converted into carbon monoxide (CO) and analyzed using the same separation and detection methods described above.[26,27] Elemental composition is reported as weight% (wt%) of the initial sample.

Boehm titrations were conducted to help identify redox-active and non-redox active oxygen-containing functional groups within the samples. This titration is commonly used to quantify acidic oxygen groups (phenol, lactone, and carboxylic groups).[25] Of the groups it can detect, only phenols are believed to be redox active and primarily associated with electron donation.[21] By subtracting the groups detected by the Boehm method from the total oxygen measured through CHN(O)S analysis, we aimed to better identify oxygen content associated with EAC. The Boehm method involves reactions of surface groups with strong bases to deprotonate the oxygen groups. Then, through an equivalence point titration with a strong acid, or through a surplus addition of acid and back-titration with another base, the deprotonated oxygen groups are quantified through comparison with reference blanks.[28] Triplicate solutions (50 mL) of sodium hydroxide (NaOH) (0.05 M, Fisher Scientific) and one sample of each of X-AC, 30 min treated $H_2O_2$-AC, and 30 min treated $HNO_3$-AC ($\sim$0.02 g) were incubated during shaking at 200 rpm for three days. Sodium hydroxide was chosen as the first base because it reacts and deprotonates phenol, lactone, and carboxylic acid groups on carbon materials.[29] An extra set of triplicate solutions without ACC was also incubated for three days to serve as a reference. Samples (10 mL) were taken from each solution, filtered, and added to 20 mL of hydrochloric acid (HCl) (0.05 M, Fisher Scientific). These samples were then titrated with sodium carbonate ($Na_2CO_3$) (0.05 M, Fisher Scientific) using an Orion Star T910 pH Autotitrator (START9100, Fisher Scientific) with an Orion ROSS Ultra pH electrode (13642237, Fisher Scientific). Once the equivalence point for each sample was reached and recorded, oxygen groups (mmol per g-AC) were quantified using eqn (3):

$$O_2 \text{ groups (mmol per g AC)} = \frac{\left(\left(V_{sample,NaOH} - V_{ref,NaOH}\right) \times \text{titer} \times C\right)_{\text{titrator base}}}{m_{ACC} \times \frac{1}{5}} \quad (3)$$

where $V_{sample,NaOH}$ (mL) is the volume of titrant used to reach the equivalence point for the titration of the experimental sample and $V_{ref,NaOH}$ (mL) is the volume of titrant used to titrate the reference blank. The concentration of the titrant ($C$, mol $L^{-1}$) and mass of sample reacting with the base ($m_{ACC}$, g) were kept constant throughout all titrations. The same titration solution ($Na_2CO_3$; 0.05 M) was used across all samples so that the titer remained constant (titer = 1). A factor of 1/5 was included to account for the amount of sample taken (10 mL) in reference to the full volume of liquid used in the sample incubations (50 mL). This method was then repeated using $Na_2CO_3$ as the reaction base to deprotonate lactone and carboxylic acid groups.[28,29] Lastly, $NaHCO_3$ was used in the final reaction base to deprotonate carboxylic acid groups.[28,29] Quantification of the acidic groups was done using the following set of equations:

$$n_{\text{carboxylic acids}} \text{ (mmol per g AC)} = \frac{\left(\left(V_{sample,NaHCO_3} - V_{ref,NaHCO_3}\right) \times \text{titer} \times C\right)_{\text{titrator base}}}{m_{ACC} \times \frac{1}{5}} \quad (4)$$

$$n_{\text{lactones}} \text{ (mmol per g AC)} = \frac{\left(\left(V_{sample,Na_2CO_3} - V_{ref,Na_2CO_3}\right) \times \text{titer} \times C\right)_{\text{titrator base}}}{m_{ACC} \times \frac{1}{5}} - n_{\text{carboxylic acids}} \quad (5)$$

$$n_{\text{phenols}}\ (\text{mmol per g AC}) = \frac{\left(\left(V_{\text{sample,NaOH}} - V_{\text{ref,NaOH}}\right) \times \text{titer} \times C\right)_{\text{titrator base}}}{m_{\text{ACC}} \times \frac{1}{5}} - \left(n_{\text{carboxylic acids}} + n_{\text{lactones}}\right) \quad (6)$$

where $V_{\text{sample,NaHCO}_3}$ and $V_{\text{sample,Na}_2\text{CO}_3}$ (mL) is the volume of titrant used to reach the pH equivalence point for these reaction bases and $V_{\text{ref,NaHCO}_3}$ and $V_{\text{ref,Na}_2\text{CO}_3}$ represent the volume of titrant needed to reach the equivalence point for the corresponding reference blanks for these reaction bases.

### 2.4 Surface area and pore volume characterization

Activated carbon cloth surface area and pore volume were characterized using density functional theory (DFT) analysis in conjunction with an Autosorb iQ (Quantachrome Corporation) instrument equipped with Quantachrome® ASiQwin™ software. A mass (0.01–0.02 g) of each AC (X-AC, 30 min treated $H_2O_2$-AC, and 30 min treated $HNO_3$-AC) was washed with DI water, dried overnight at 70 °C, and inserted into 9 mm Autosorb columns. The samples were then outgassed for ~12 hours at 200 °C using the two outgassing stations on the instrument. Surface area and cumulative pore volume data were then obtained from $N_2$ adsorption/desorption isotherm data (40 adsorption/20 desorption data points) in the relative pressure range from $10^{-7}$ to 1 bar at −196 °C. Density functional theory was then used to calculate pore volumes and sample surface area.

### 2.5 Statistical analysis

RStudio was used to conduct the statistical analyses, utilizing two-way analysis of variance (ANOVA) coupled with Tukey testing and linear regression fitting commands. For these analyses, $p < 0.05$ was considered significant. ANOVA/Tukey tests were conducted to establish significance between quantified EAC/EDC data, predicted *vs.* observed EAC values, chemical property data obtained from XPS and the Boehm titration, and physical property analysis of surface areas and cumulative pore volumes between the non-treated and treated materials. Linear regression fitting was conducted to establish significance in the correlation analysis between electron exchange capabilities and physical/chemical properties and for parity plot analysis comparing predicted EAC *vs.* observed EAC values.

## 3. Results and discussion

Our overarching goal was to evaluate strategies to increase PCM electron exchange rates and capacities over short time scales. To achieve this goal, we used an ACC obtained from a highly pure feedstock (novoloid phenol-aldehyde fiber) and created a set of ACCs with different chemical and physical properties through immersion in chemical oxidants ($H_2O_2$ or $HNO_3$).[30] We then quantified their short-term EACs, EDCs, and electron accepting rates using a mediated electrochemical method. Finally, we developed relationships between the electron exchange metrics and physical (surface area, pore volume) and chemical (oxygen content) properties to understand underlying reasons for changes in electron exchange behavior.

### 3.1 Electron accepting capacities

We first conducted MER tests on the treated AC cloths ($H_2O_2$-AC and $HNO_3$-AC) and compared them to an non-treated AC cloth (X-AC). Prior studies have studied EEC for as long as multiple months.[9] Here we focused on short time scales of up to a maximum of 5–6 hours.[9] Within that time period, X-AC had an average short-term total EAC of 1.80 ± 0.13 mmols $e^-$ per g-AC (Fig. 1). This value is substantially larger than previously published EACs of biochars (~0.1–0.6 mmols $e^-$ per g-PCM) measured over timescales ranging from hours to >60 days, though it is comparable to reported EACs of granular AC (GAC) (~0.5–1.7 mmols $e^-$ per g-AC) measured under unspecified timescales.[9,19,31] The larger values found here could be associated with the larger surface area (on a per gram basis) of the AC cloth (>1000 $m^2$ $g^{-1}$ Kynol AC; ≤500 $m^2$ $g^{-1}$ biochar), which provides a larger reactive surface area as well as the fact that the AC used in this study was an engineered material of high purity and low ash content. Ash content is typically higher when natural materials such as wood are the feedstock. Ash content can be associated with lower EECs due to pore blockage, potentially limiting access to reactive sites and hindering mediator diffusion.[9,19,30,32]

Treatment with $H_2O_2$ for 2 min resulted in a significant increase ($p < 0.05$; relative to X-AC) of EAC to 2.45 ± 0.10 mmols-$e^-$ per g-AC over a 2–3 hour period. Extending $H_2O_2$ treatment from 2 and 5 min to 30 min significantly increased EAC, while results for the 2 and 5 min incubations were statistically similar ($p = 0.056$). Treatment for 24 hour resulted in an insignificant increase in EAC relative to the 30 min treatment ($p = 0.62$; 3.35 ± 0.13 mmols-$e^-$ per g-AC; Fig. S2), indicating that 30 min was sufficient to produce a near maximum EAC over the 3–4 hour period examined.

Treatment with $HNO_3$ resulted in the largest increase in EAC relative to X-AC. The EAC increased by 3.4 times after a 30 s $HNO_3$ incubation to 6.20 ± 0.05 mmols-$e^-$ per g-AC. Five and 30 min $HNO_3$ treatments increased EAC further to a max of

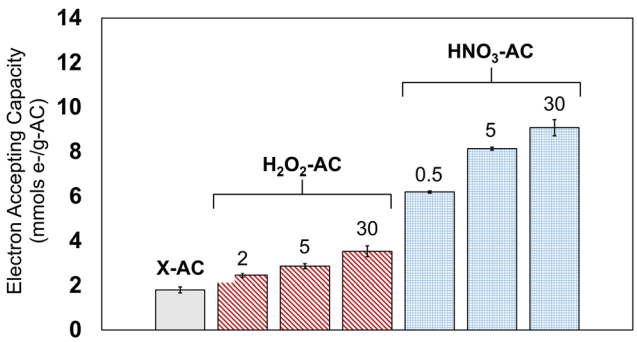


Fig. 1 Average electron accepting capacities of non-treated (X-AC), $H_2O_2$-treated, and $HNO_3$-treated ACCs. Numbers above individual bars represent the amount of time (minutes) the ACCs were incubated in their corresponding chemicals. Error bars represent the standard error of triplicates.

9.16 ± 0.36 mmols-e$^-$ per g-AC (30 min treatment; 5.1 times that of X-AC). Similar to the $H_2O_2$ treatments, the 24-hour treatment with $HNO_3$ produced an insignificant increase ($p$ = 0.98; 9.4 ± 1.3 mmols-e$^-$ per g-AC) compared to the 30 min treatment. Collectively these results show a strong dependence of PCM short-term EAC on chemical type and duration of treatment.

$H_2O_2$ and $HNO_3$ treatment of PCMs has been reported in prior studies, wherein slight or substantial increases were seen in electron exchange, however these short-term EACs are larger than many EACs reported over longer or unknown time periods.[9,20,23] Typically EACs are measured over the course of hours, days, or under unspecified timescales.[15,19] For example, Prévoteau *et al.*[9] reported biochar EACs in the range of 0.05–0.4 mmols e$^-$ per g-PCM measured over a 66 day period. Additionally, Klüpfel *et al.*[19] reported biochar EAC values in the range of 0.25–0.91 mmols e$^-$ per g-PCM under similar MER testing conditions. AC samples however, have been shown to reach much higher values compared to other PCMs, with a maximum EAC of ~6 mmols e$^-$ per g-AC reported in one study for an $HNO_3$ treated GAC, although the timescale was unreported.[31] The EAC values obtained here, which reach values higher than those reported elsewhere, demonstrate that large EACs can be achieved under relatively short timescales.[9,19,20] EECs can vary widely amongst the different types of PCMs, as mentioned above. Our findings display the equal importance of reporting timescale measurement for comparison across PCM redox capacity studies.

### 3.2 Electron accepting kinetics

The rate of electron transfer to the ACCs depended on the treatment and timepoint during the EAC tests (Fig. 2). Within the first 30 minutes, X-AC accepted 0.95 ± 0.01 mmols e$^-$ per g-AC. Across the $H_2O_2$-AC and $HNO_3$-AC samples, roughly 1.5–2.0 times and 3.3–3.5 times more electrons were accepted, respectively, relative to X-AC, indicating a much faster initial electron transfer rate with treatment. Across all materials, the 30 min treated $HNO_3$-AC had the highest electron transfer rate of 0.11 ± 0.02 mmols e$^-$ per g-AC per min within the first 30 minutes. For the remainder of the 1.5 hour period, X-AC had an average electron transfer rate of 0.005 ± 0.0008 mmols e$^-$ per g-AC per min as determined from the slope of the linear trend line from timepoints 0.5–1.5 hours. (Fig. S3–S5). Interestingly, compared to X-AC, the average electron transfer rate in 30 min treated $H_2O_2$-AC sample, while substantially larger across the first 30 min of monitoring, increased only slightly across the period of 0.5–1.5 hours (0.009 ± 0.0009 mmols e$^-$ per g-AC per min). $HNO_3$-ACs had a much larger rate across this same period, with the maximum of 0.042 ± 0.006 mmols e$^-$ per g-AC per min revealed in the 30 min treated samples. While the 30 min treated samples exhibited the largest rates during the 0.5–1.5 hour period of monitoring in both $H_2O_2$- and $HNO_3$-AC samples, variations in rate were evident based on treatment time. Although $H_2O_2$-AC EAC rates were similar between the 2 and 5 min treated samples (Fig. S4), a large degree of variation was seen across all $HNO_3$-AC samples (Fig. S5).

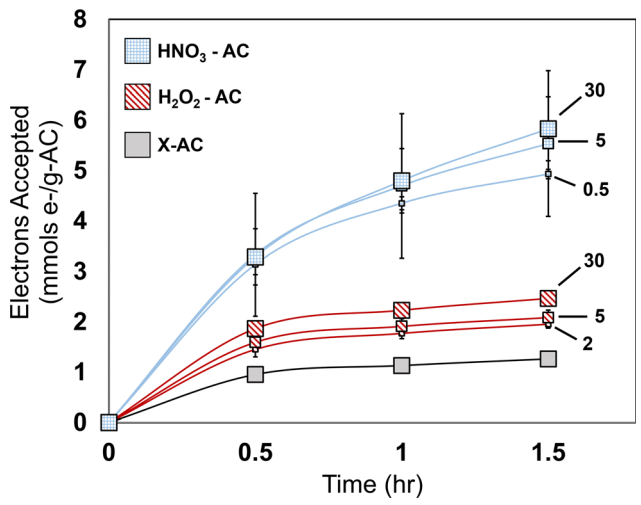


Fig. 2 Electron accepting capacity as a function of time for X-AC, $H_2O_2$-AC, and $HNO_3$-AC. Numbers attached to the individual lines represent the amount of time (minutes) the ACCs were incubated in their corresponding chemicals. Error bars represent the standard error of triplicates.

Many PCM-focused studies have reported total EACs, but kinetic information is commonly unreported.[9,19,20] Some of the only EEC rates to date were reported by Prévoteau *et al.*[9] wherein EDC rates reached as high as 0.1 mmols e$^-$ per g-PCM per hour. Sun *et al.*[3] provided some quantitative data for electron transfer rate constants to demonstrate kinetic differences between direct carbon matrix and functional group electron transfer pathways. Across the majority of PCM-focused studies, less attention has been given towards timescale tracking of EEC rates. The accelerated EAC rate changes revealed here have implications for applications in which short reaction times are desired. Additionally, the enhancements seen here may prove relevant for electrocatalytic systems (*e.g.* oxygen or hydrogen evolution reactions), an area that could serve as the basis for future studies.[33,34] Across the first 30 minutes of monitoring, $HNO_3$-AC reached a maximum of 3.33 ± 1.22 mmols e$^-$ per g-AC accepted, a value ~1.8 times that of the total short-term EAC of X-AC. By monitoring the rates and timescales in this study, we find that large differences can occur not only in PCM short-term total electron acceptance, but also in the rate of PCM electron acceptance resulting from chemical oxidative treatment.

### 3.3 Electron donating capacities

One possible explanation for the increased EAC after the chemical treatments is that electrons stored in the X-AC cloths were removed by the chemical oxidants. PCMs can naturally store electrons, even if they are not reduced chemically or electrochemically.[35,36] The EDC of non-treated PCMs are in the range of 0–7.0 mmols e$^-$ per g-PCM, with values in the range of 0.1–1 mmols e$^-$ per g-PCM over time periods on the scale of hours.[9] It is plausible that oxidants, such as $H_2O_2$ and $HNO_3$, can extract pre-existing electrons within PCMs by modifying redox-active sites and effectively impacting the distribution of oxygen functionalities.[37,38] We conducted MEO tests on

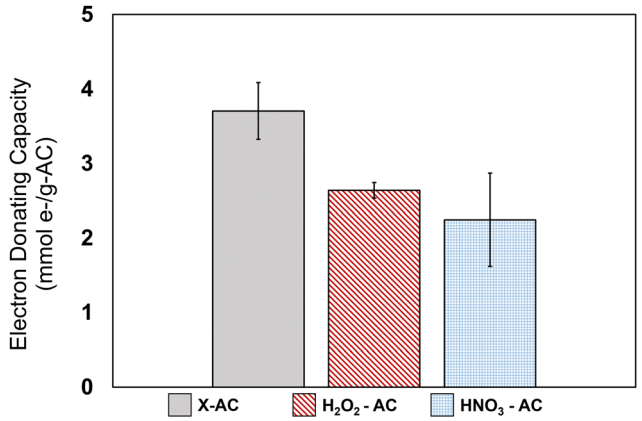


Fig. 3 Average electron donating capacities of 30-minute treated X-AC, $H_2O_2$-AC, and $HNO_3$-AC. Error bars represent the standard error of triplicates.

the X-AC and 30 min treated $H_2O_2$-AC and $HNO_3$-AC cloths on roughly the same timescale used in the EAC tests (Fig. 3). The X-AC had an EDC of 3.71 ± 0.38 mmols $e^-$ per g-AC, which is larger compared to previously reported EDCs and it is almost double the EAC of the X-AC.[39,40] Treatment with either of the chemical oxidants resulted in a significant decrease ($p < 0.05$) in EDC relative to X-AC. The difference in EDC between the $H_2O_2$ and $HNO_3$ treated samples was not significant ($p = 0.53$). $H_2O_2$-treated AC resulted in an EDC of 2.64 ± 0.10 mmols $e^-$ per g-AC whereas the $HNO_3$-treated samples had an EDC of 2.26 ± 0.63 mmols $e^-$ per g-AC. The difference in EDC between the X-AC and the $H_2O_2$-AC and $HNO_3$-AC samples was approximately 1.07 and 1.46 mmols $e^-$ per g-AC, respectively. This loss of previously stored electrons accounts for only ~62% and 20% of the resulting EAC of the $H_2O_2$-AC and $HNO_3$-AC samples, respectively. Therefore, a decrease in stored electrons prior to the EAC tests due to the chemical oxidants might explain some of the increase in EACs but it does not explain the majority of the increase.

### 3.4 Chemical properties of the non-treated and treated ACCs

Since $H_2O_2$ and $HNO_3$ are oxidizing chemicals that influence the surface chemistry of PCMs, we used x-ray photoelectron spectroscopy (XPS) to determine if the treatments resulted in the emergence of new oxygen-containing functional groups that could help explain the increased EAC.[1,41] We only studied samples subjected to 30 min treatments because those tests resulted in the most substantial changes in EAC relative to the non-treated control. Carbon (C) 1s and oxygen (O) 1s peaks were confirmed in X-AC based on the binding energies centered at ~285 eV and ~530 eV, respectively (Fig. S6).[42–45] Surveys of the $H_2O_2$-AC and $HNO_3$-AC samples were similar to those of X-AC, but with increases in the O 1s peaks and decreases in the C 1s peaks. The calculated total oxygen percentages for X-AC, $H_2O_2$-AC, and $HNO_3$-AC samples were 4.42 ± 0.36 at%, 11.47 ± 2.75 at% and 11.67 ± 3.61 at%, respectively (Fig. 3A). The increase in O content with treatment was expected. Li *et al.*[1] showed an almost identical increase in oxygen (from 3.62% to 11.34%) after treating AC fiber with 30% $H_2O_2$ for 16 hours. Similarly, Mangun *et al.*[41] reported oxygen percentages of 5.84 at%, 9.95 at%, and 12.77 at% for X-AC fiber, 30% $H_2O_2$ treated, and concentrated $HNO_3$-treated, respectively.

Deconvolution of the oxygen peaks to help identify putative functional groups did not yield a clear trend across the treatments (Fig. 4B). Rather than select individual functionalities, classes of oxygen-containing functional groups were chosen to help mitigate error in the deconvolution process. The classes selected were aromatic and aliphatic groups containing C═O bonds (*e.g.*, quinones, ketones), and aliphatic groups containing a C═O bond as well as an additional C–O bond (*e.g.*, ketones, ethers) because these groups have been implicated in electron exchange.[23,46–48] Deconvolution revealed small differences in the oxygen content present across samples. Aromatic C═O groups had the largest presence in both the X-AC and $H_2O_2$-AC samples, whereas $HNO_3$-AC oxygen content was predominately comprised of aliphatic C═O groups. Based on prior findings, it was expected that significant increases would be found for aromatic C═O groups across both treatments.[41] While our findings were consistent in the case of $H_2O_2$-AC samples, a slight decrease was found in the $HNO_3$-AC samples for these groups. The lack of a clear or consistent trend may have been due to the deconvolution process itself (error and misinterpretation can occur when attempting to identify functionalities that may have very similar binding energies[49]) but also because XPS is strictly a surface analysis tool and does not examine the chemical moieties present within the pore structure.[49]

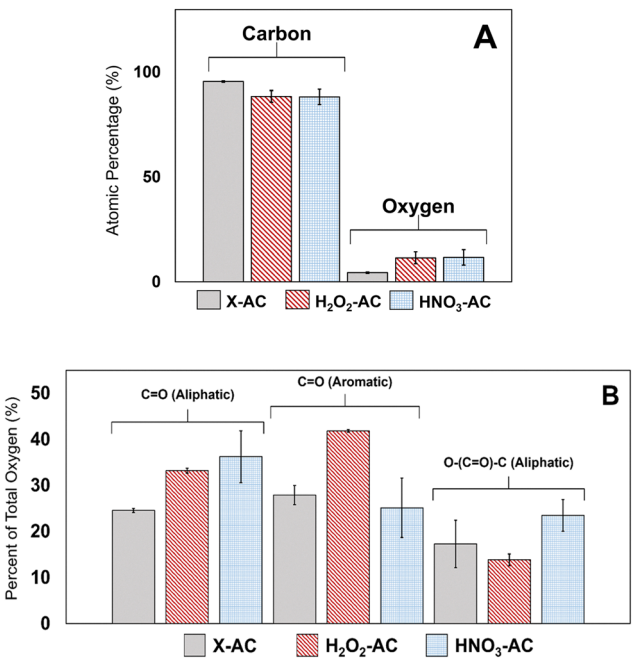


Fig. 4 (A) Atomic percentage of carbon and oxygen on the surface of the X-AC, $H_2O_2$-AC, and $HNO_3$-AC. (B) Major carbon and oxygen-containing surface functional groups on the X-AC and treated ACCs ($H_2O_2$-AC and $HNO_3$-AC) identified using XPS. Error bars represent the standard error of triplicates.

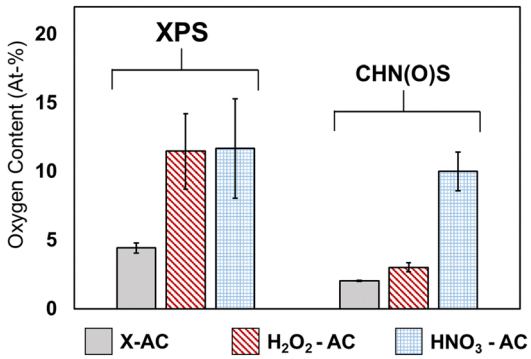


Fig. 5 Comparison of sample oxygen content (at%) collected from XPS and CHN(O)S analysis for X-AC, 30 min treated $H_2O_2$-AC, and 30 min treated $HNO_3$-AC. Standard deviation represents the standard error of duplciates in CHN(O)S and triplicates in XPS.

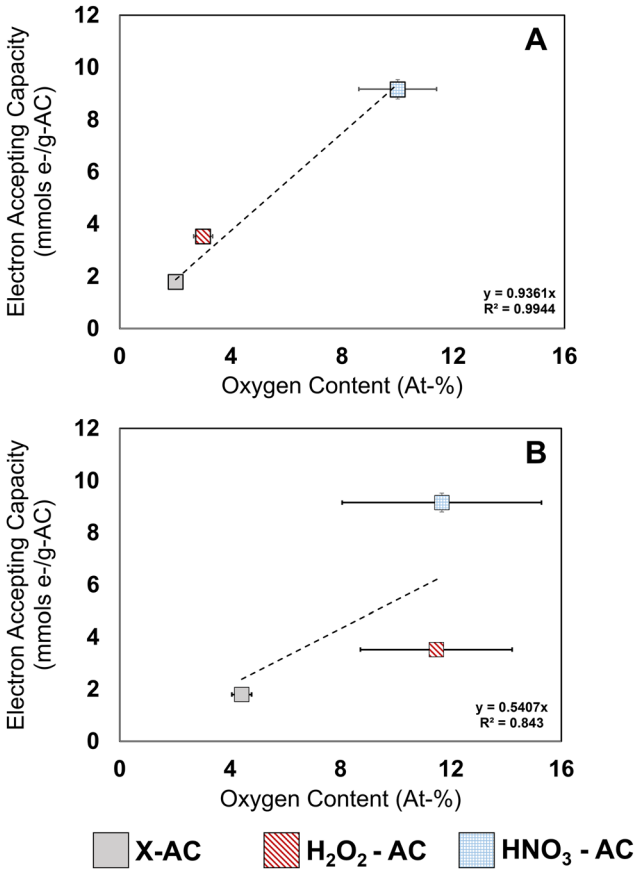


Fig. 6 PCM electron accepting capacity as a function of material oxygen content obtained from (A) CHN(O)S analysis and (B) XPS analysis. Error bars represent the standard error of triplicates (EAC/XPS) or duplicates (CHN(O)S).

To understand elemental composition within the cloths and not just the surface, CHN(O)S analysis was conducted on X-AC as well as the 30 min treated $H_2O_2$-AC and $HNO_3$-AC samples (Table S1). For some samples, the data obtained from CHN(O)S analysis differed from that obtained from XPS analysis (Fig. 5). CHN(O)S values were lower than their XPS counterparts, but only significantly lower ($p < 0.05$) for X-AC and $H_2O_2$-AC. X-AC and 30 min treated $H_2O_2$-AC and $HNO_3$-AC CHN(O)S oxygen content values were 2.01 ± 0.04 at%, 3.00 ± 0.34 at%, and 10.0 ± 1.40 at%, respectively. While X-AC and $HNO_3$-AC differed by roughly 2.41% and 1.67%, respectively, between the two analysis types, the greater differences were seen in the $H_2O_2$-AC samples with a difference of ~8.47%. These differences help provide mechanistic insight into how the treatments affected the location of new oxygen functional groups. Since the XPS results (surface-level analysis) were in closer agreement with the CHN(O)S analysis (surface plus interior analysis) for the X-AC and $HNO_3$-AC materials, we conclude that there was higher uniformity in the distribution of oxygen functionalities on the outer and inner surface of those materials. In contrast for $H_2O_2$-AC, the much larger difference across these methods indicates that treatment with $H_2O_2$ resulted in creation of oxygen functional groups primarily on the outer rather than inner surface.

Based on the CHN(O)S analysis, we calculated two elemental ratios that have been associated with redox behavior. O/C and H/C ratios indicate potential drivers of electron transfer.[3,19] Sun *et al.*[3] indicated that electron transfer was dominated by direct transfer across the carbon matrix (*e.g.* electron conduction) for materials possessing both low H/C and O/C values (~0.35 and ~0.09, respectively). At higher O/C ratios, the contribution of surface functional groups to electron exchange increased, resulting in a decrease in exchange rate.[3] The H/C values, calculated from wt% averages, of X-AC, 30 min treated $H_2O_2$-AC, and 30 min treated $HNO_3$-AC samples ranged from 0.0036–0.0059. The minimal differences across H/C ratios indicate little to no change in electrical conductivity capabilities across the treatments.[3] The O/C ratios, however, were significantly different (0.029–0.16 wt%; $p < 0.05$). These results support a greater role of surface functional group changes than electron conduction changes to the electron transfer differences seen in our ACC materials.

Correlation plots between EAC and oxygen content obtained from the two methods were compared to determine if one method had stronger predictive power of EAC (Fig. 6). The oxygen content obtained from XPS analysis exhibited a moderate correlation with EAC ($R^2$ = 0.84, $p$ = 0.51), whereas oxygen content from CHN(O)S analysis correlated strongly with EAC ($R^2$ = 0.99, $p < 0.05$). It is important to note that not all oxygen content captured through both methods participates in electron exchange. Nevertheless, our results show a much stronger relationship between EAC and the oxygen content based on CHN(O)S analysis compared to XPS. Prior studies that evaluated similar correlations showed good predictive power of oxygen content based on XPS data. In those studies, biochar was analyzed. Biochar has a small surface area (<150 $m^2\ g^{-1}$) and pore volume (<0.1 mL $g^{-1}$) compared to the ACC in this study.[50] Comparison of carbon and oxygen contents (wt%) obtained from CHN(O)S and XPS analyses of low surface area biochars showed almost identical results between the analyses

types.[51] We hypothesize that our findings differ from studies on biochar because of the large pore volumes and deep internal surface areas of the ACCs that are best probed using bulk sample analysis like CHN(O)S rather than XPS.

To probe more deeply into the relationships between the redox-active portion of oxygen groups measured *via* CHN(O)S analysis, we subtracted off non-redox groups measured using the Boehm titration. The Boehm titration quantifies a mix of redox (phenols; primarily electron donors) and non-redox-active (carboxylic acids + lactones) acidic oxygen containing functional groups.[21] The difference between these groups and those quantified *via* CHN(O)S analysis can give better insight into the presence of oxygen species capable of accepting electrons.[28,29] We conducted the titrations on the 30 min treated X-AC, $H_2O_2$-AC, and $HNO_3$-AC samples. The total acidic oxygen content was slightly lower than the total oxygen content measured by CHN(O)S analysis (Fig. 7). After converting the CHN(O)S oxygen content units (eqn (S2)) to those from the Boehm titration, the Boehm results were subtracted from these values. We hypothesize that the difference represents putative redox-active functional groups that could accept electrons. The quantity of these functional groups were 0.76 ± 0.14, 0.81 ± 0.35, and 4.59 ± 1.22 mmols-O per g-AC for X-AC, 30 min treated $H_2O_2$-AC, and 30 min treated $HNO_3$-AC, respectively.

Assuming each mmol of these redox-active oxygens could accept 2 mmols electrons,[52,53] we calculated predicted EACs of 1.53 ± 0.29, 1.61 ± 0.70, and 9.17 ± 2.45 mmols $e^-$ per g-AC for X-AC, 30 min treated $H_2O_2$-AC, and 30 min treated $HNO_3$-AC, respectively. Based on a parity plot comparing the predicted EACs to our observed EACs (Fig. 8), we saw strong agreement for the X-AC and $HNO_3$-AC samples. However, the $H_2O_2$-AC values fell below the 1 : 1 line, indicating that the predicted values were lower than the observed EAC. The good agreement for the X-AC and $HNO_3$-AC samples are likely due to quinones contributing to the majority of the putative redox-active oxygen groups. Quinones have been well characterized in PCMs. They are reduced through a two electron reaction.[52,53] These groups have been implicated in PCM electron exchange activity, given their redox reversible nature.[54,55] On carbon materials, $HNO_3$ oxidation results in the formation of both basic and acidic functional groups, including carbonyls, carboxylic acids, phenols, *etc.*, *via* reactions with aromatic rings present within carbon and oxidative ions such as $NO_3^-$.[51] Gerber *et al.*[56] found that in the early stage oxidation (0–1 hour) of carbon nanotubes by $HNO_3$, deposited oxygen containing functional groups were primarily quinones and phenols. Our 30 min treated $HNO_3$-AC samples are consistent with this finding given the large presence of phenol groups revealed *via* the Boehm titration, which would not accept electrons, (Fig. S10), and the increased electron accepting activity revealed in MER analysis, potentially due to quinone deposition.

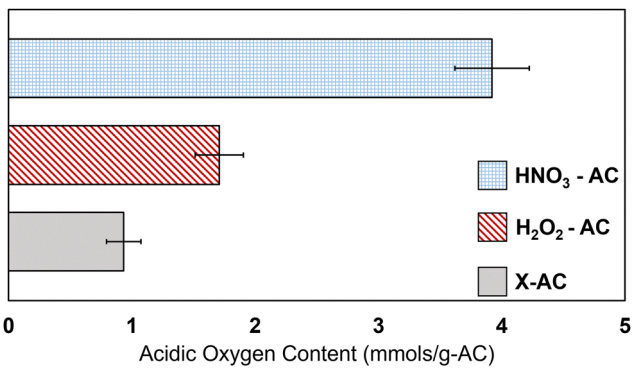


Fig. 7 Boehm titration results revealing the total acidic oxygen content for X-AC, 30 min treated $H_2O_2$-AC, and 30 min treated $HNO_3$-AC. Error bars represent the standard error of triplicates.

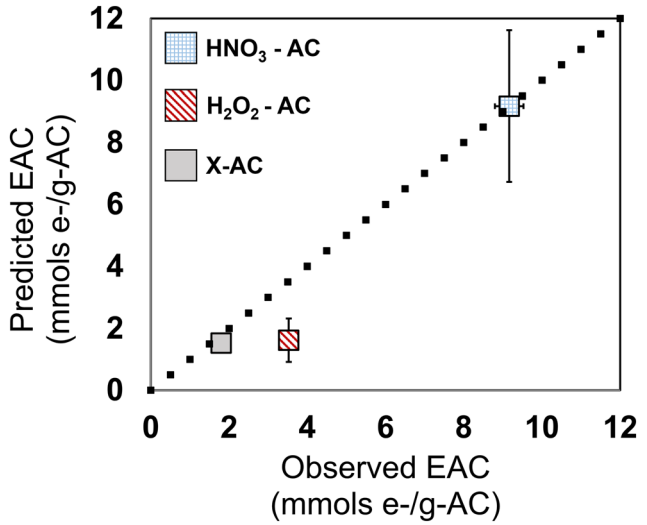


Fig. 8 Parity plot comparison of predicted EAC calculated from Boehm titration and CHN(O)S data and observed EAC obtained from MER experimentation. Error bars represent the standard error of triplicates.

The under-prediction in the $H_2O_2$-AC indicates the potential instability of oxidation by $H_2O_2$ over long time periods. MER, XPS, and Boehm titration data were collected within 24–48 hours of $H_2O_2$ treatment, leaving little time for any natural decomposition or loss of surface oxygen content. However, CHN(O)S analysis was outsourced, resulting in a large gap (>1 month) between treatment and analysis. It has been reported that AC surface oxygen groups deposited *via* $H_2O_2$ treatment decompose significantly over a timescale of >50 days.[57] Therefore, it is plausible that some redox-active surface groups formed *via* $H_2O_2$ treatment (*e.g.* peroxy groups), while increasing EAC in the short term, may not be stable in the long term.[58] Further, it has been established that AC materials can decompose hydrogen peroxide resulting in the formation of water ($H_2O$) and oxygen gas ($O_2$).[59] It is also known that AC materials can adsorb $O_2$ (another potential electron sink during MER), though it is readily removed through thermal methods.[60] Given the drying step performed prior to CHN(O)S analysis, as described above, it is possible that the EAC under prediction is due to loss/displacement of previously adsorbed oxygen gas which could have theoretically accepted electrons during the EAC tests.[61] Towards establishing some validity to these claims, we mimicked the drying process conducted prior to CHN(O)S analysis and allowed extended time to pass

(~1.5 weeks) before MER analysis of our 30 min treated $H_2O_2$-AC sample. Between these samples, and our original data, we found a slight decrease in EAC as well as a higher degree of fluctuation across our replicates (Fig. S11). Although not statistically significant ($p = 0.056$) these results show the potential for decrease in $H_2O_2$ deposited oxygen containing functional groups, even over a shorter time-period.

### 3.5 Physical properties of the non-treated and treated cloths

To understand changes in PCM physical characteristics resulting from chemical treatment and to determine any potential relationships with electron exchange kinetics and capacities, we compared the cumulative pore volumes and surface areas of our materials before and after the chemical treatments (Fig. 9).

We evaluated the surface area and pore volume of our ACCs because these properties influence accessibility and abundance of reactive sites. The X-AC had a cumulative pore volume of 0.626 ± 0.016 mL $g^{-1}$ and a total surface area of 1518.5 ± 10.5 $m^2$ $g^{-1}$, which are consistent with previous reports.[35,40] Treatment with $H_2O_2$ for 2 min resulted in pore volume and surface area values of 0.612 ± 0.006 mL $g^{-1}$ and 1512.9 ± 12.9 $m^2$ $g^{-1}$ respectively, indicating essentially no change ($p > 0.05$). Conversely, the 30 min treatment resulted in a significant decrease ($p < 0.05$) in both cumulative pore volume (0.576 ± 0.006 mL $g^{-1}$) and surface area (1428.8 ± 11.3 $m^2$ $g^{-1}$). The 0.5 min treated $HNO_3$-AC sample had pore volume and surface area values of 0.529 ± 0.006 mL $g^{-1}$ and 1348.7 ± 9.21 $m^2$ $g^{-1}$, respectively, which further decreased to 0.472 ± 0.001 mL $g^{-1}$ and 1264.5 ± 10.4 $m^2$ $g^{-1}$, respectively, after the 30 min treatment. Of the total "lost" pore volume, roughly 67% and 63% could be attributed to micropore (0–2 nm width) loss in $H_2O_2$-AC and $HNO_3$-AC samples, respectively (Table S1). These findings are consistent with previous studies that have used oxidative techniques. For example, Li *et al.*[1] reported a surface area decrease from 1480 $m^2$ $g^{-1}$ to 1350 $m^2$ $g^{-1}$ for AC fiber after soaking in 30% $H_2O_2$. Although additional physical characteristics such as mechanical strength were not directly measured, no apparent physical integrity changes were observed in our ACCs. Mechanical durability may, however, warrant consideration for future works wherein direct applications for flow-through or variable hydrodynamic systems are studied. Additionally, physical characteristics such as hydrophobicity should also be considered in future studies due to its role in material and pore wettability.[62]

Collapsing small pores and building new connectivity across and within internal pore networks could have contributed to the improved electron accepting kinetics and capacities observed in our EAC tests. Microscale pores have been implicated in slowing the diffusion of mediators towards reactive sites during mediated electrochemical tests.[19,47] Increasing the size of those pores can therefore accelerate transfer of mediators in and out of the ACC. Our results showing that the $HNO_3$-AC had the highest electron transfer rates but smallest micropore volume support this hypothesis. Additionally, previously inaccessible moieties may become available as isolated pores are opened, resulting in higher EECs.[4,15,19] Our finding that EAC was negatively correlated with surface area is not consistent with many prior studies, but is logical considering the chemical treatments used in this study.[47,63] The chemicals changed multiple properties at the same time, including oxygen content, surface area, and pore volume, but they most strongly impacted oxygen content. Oxygen content increased upwards of four-fold, whereas the largest decrease in surface area was only approximately 17%. Prior studies often cite the development of oxygen-containing functional groups alongside an increase in surface area, where the combination of those two properties were the likely reason for increased electron exchange.[47,63] While the collapse of micropores likely aided in small part in increasing EAC rate and short-term total EAC through enhanced internal conductivity and access to inherent or newly formed redox-active oxygen sites, the primary mode of action for the chemical oxidants is increased oxygen content. This, alongside the fact that these materials maintained a strong conductive carbon matrix (low H/C ratios) across the treatments, highlights that oxygen content is the primary factor associated with increased short-term EAC rates and total in these tests and that large surface area alone is not necessarily critical for increasing EAC. Alkaline treatments (*e.g.* KOH, NaOH) have also been shown to increase porosity and defects in PCMs.[64,65] These, and other alkaline solvents, could be utilized for further analysis of the impact porosity expansion on PCM electron exchange while potentially minimizing redox-active functional group interference.[64]

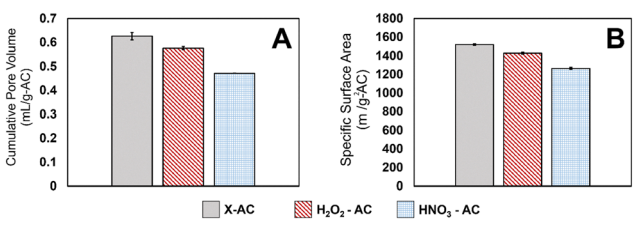


Fig. 9 Physical property results for 30-minute treated X-AC, $H_2O_2$-AC, and $HNO_3$-AC. (A) Cumulative pore volumes for non-treated and treated materials. (B) Specific surface area values for non-treated and treated materials. Error bars represent the standard error of three replicates.

## 4. Conclusions

Our overall objective was to develop PCMs with faster electron exchange and higher electron acceptance over short time periods (<6 hours). We soaked activated carbon cloths (ACCs) in the chemical oxidants $H_2O_2$ and $HNO_3$ to alter the material properties. We determined the impact of chemical treatment on short-term electron transfer kinetics and total electron accepting capacity (EAC) through examining the relationships between these performance metrics and oxygen content, oxygen-containing functional groups, surface area, and pore volume. Our major findings are:

- Treatment with $HNO_3$ ($HNO_3$-AC) for 30 min resulted in the largest EAC increase relative to the non-treated AC (5.1×)

over a 5–6 hour incubation. Treatment with hydrogen peroxide ($H_2O_2$-AC) also resulted in significant EAC increases, reaching a maximum of 1.9× relative to the non-treated AC.

• The kinetics of electron transfer increased with each treatment in the first 30 minutes. Afterwards, the rates for X-AC and $H_2O_2$-AC were similar for the remaining hour. The $HNO_3$-AC exhibited the highest rates throughout the entire test.

• Total oxygen content increased due to $H_2O_2$ and $HNO_3$ treatment as revealed by XPS analysis, CHN(O)S analysis, and the Boehm titration. Oxygen content obtained *via* CHN(O)S had the strongest correlation with EAC, highlighting the potential limitations of XPS analysis on materials with deep internal surface area and porosity.

• EAC values predicted based on the subtraction of non-redox active oxygen content (Boehm titration data) from total oxygen content (CHN(O)S data) agreed well with observed EAC values in X-AC and $HNO_3$-AC samples, but not in $H_2O_2$-AC samples. The under-prediction in $H_2O_2$-AC samples is likely due to decomposition of some oxygen-containing surface groups over time.[57]

• EAC increased significantly with each treatment despite decreases in surface area and pore volume, a finding most apparent in the $HNO_3$-AC samples. These results, although contrary to correlations drawn between EAC and PCM physical characteristics in previous studies, are logical considering the large increase in oxygen content as well as the increased access of mediators to reactive sites caused by micropore collapse/widening.

## Conflicts of interest

The authors declare no conflicts of interest.

## Data availability

The authors confirm that the data supporting the findings can be found within the article and in the included supplementary information (SI). Supplementary information: equations, tables, and figures encompassing additional data not included in the main text. See DOI: **https://doi.org/10.1039/d5ma00727e**.

## Acknowledgements

This material is based upon work supported by the National Science Foundation under Grant No. 1944191. XPS was carried out at the analytical instrumentation facility (AIF) at North Carolina State University. CHN(O)S analysis was carried out by Measurlabs testing facility in Helsinki, Finland.

## References

1 L. Li, P. A. Quinlivan and D. R. U. Knappe, Effects of activated carbon surface chemistry and pore structure on the adsorption of organic contaminants from aqueous solution, *Carbon*, 2002, **40**, 2085–2100.
2 B. Qiu, Q. Shao, J. Shi, C. Yang and H. Chu, Application of biochar for the adsorption of organic pollutants from wastewater: modification strategies, mechanisms and challenges, *Sep. Purif. Technol.*, 2022, **300**, 121925.
3 T. Sun, B. D. A. Levin, J. J. L. Guzman, A. Enders, D. A. Muller, L. T. Angenent and J. Lehmann, Rapid electron transfer by the carbon matrix in natural pyrogenic carbon, *Nat. Commun.*, 2017, **8**, 14873.
4 L. Yu, Y. Yuan, J. Tang, Y. Wang and S. Zhou, Biochar as an electron shuttle for reductive dechlorination of pentachlorophenol by Geobacter sulfurreducens, *Sci. Rep.*, 2015, **5**, 16221.
5 J. Ai, H. Ma, D. J. Tobler, M. C. Mangayayam, C. Lu, F. W. J. Van Den Berg, W. Yin and H. C. Bruun Hansen, Bone Char Mediated Dechlorination of Trichloroethylene by Green Rust, *Environ. Sci. Technol.*, 2020, **54**, 3643–3652.
6 Y. Lu, Q. Xie, L. Tang, J. Yu, J. Wang, Z. Yang, C. Fan and S. Zhang, The reduction of nitrobenzene by extracellular electron transfer facilitated by Fe-bearing biochar derived from sewage sludge, *J. Hazard. Mater.*, 2021, **403**, 123682.
7 J. Yang, B. Pan, H. Li, S. Liao, D. Zhang, M. Wu and B. Xing, Degradation of *p*-Nitrophenol on Biochars: Role of Persistent Free Radicals, *Environ. Sci. Technol.*, 2016, **50**, 694–700.
8 M. Chu, W. Tian, J. Zhao, M. Zou, Z. Lu, D. Zhang and J. Jiang, A comprehensive review of capacitive deionization technology with biochar-based electrodes: biochar-based electrode preparation, deionization mechanism and applications, *Chemosphere*, 2022, **307**, 136024.
9 A. Prévoteau, F. Ronsse, I. Cid, P. Boeckx and K. Rabaey, The electron donating capacity of biochar is dramatically underestimated, *Sci. Rep.*, 2016, **6**, 32870.
10 Technology Screening Matrix|Federal Remediation Technologies Roundtable (FRTR), **https://frtr.gov/matrix/Water-Treatment-Technologies/**, (accessed 29 October 2025).
11 T. Wirthensohn, P. Schoeberl, U. Ghosh and W. Fuchs, Pilot plant experiences using physical and biological treatment steps for the remediation of groundwater from a former MGP site, *J. Hazard. Mater.*, 2009, **163**, 43–52.
12 J. Y. Tian, Z. L. Chen, H. Liang, X. Li, Z. Z. Wang and G. B. Li, Comparison of biological activated carbon (BAC) and membrane bioreactor (MBR) for pollutants removal in drinking water treatment, *Water Sci. Technol.*, 2009, **60**, 1515–1523.
13 R. S. Gabhi, D. W. Kirk and C. Q. Jia, Preliminary investigation of electrical conductivity of monolithic biochar, *Carbon*, 2017, **116**, 435–442.
14 V. Hoffmann, C. Rodriguez Correa, D. Sautter, E. Maringolo and A. Kruse, Study of the electrical conductivity of biobased carbonaceous powder materials under moderate pressure for the application as electrode materials in energy storage technologies, *GCB Bioenergy*, 2019, **11**, 230–248.
15 L. Yu, Y. Wang, Y. Yuan, J. Tang and S. Zhou, Biochar as Electron Acceptor for Microbial Extracellular Respiration, *Geomicrobiol. J.*, 2016, **33**, 530–536.
16 D. R. Lobato-Peralta, P. U. Okoye and C. Alegre, A review on carbon materials for electrochemical energy storage

applications: state of the art, implementation, and synergy with metallic compounds for supercapacitor and battery electrodes, *J. Power Sources*, 2024, **617**, 235140.
17 J. M. Saquing, Y.-H. Yu and P. C. Chiu, Wood-Derived Black Carbon (Biochar) as a Microbial Electron Donor and Acceptor, *Environ. Sci. Technol. Lett.*, 2016, **3**, 62–66.
18 L. Liu, G. Liu, J. Zhou, J. Wang, R. Jin and A. Wang, Improved bioreduction of nitrobenzene by black carbon/biochar derived from crop residues, *RSC Adv.*, 2016, **6**, 84388–84396.
19 L. Klüpfel, M. Keiluweit, M. Kleber and M. Sander, Redox Properties of Plant Biomass-Derived Black Carbon (Biochar), *Environ. Sci. Technol.*, 2014, **48**, 5601–5611.
20 F. J. Chacón, M. A. Sánchez-Monedero, L. Lezama and M. L. Cayuela, Enhancing biochar redox properties through feedstock selection, metal preloading and post-pyrolysis treatments, *Chem. Eng. J.*, 2020, **395**, 125100.
21 N. Walpen, G. J. Getzinger, M. H. Schroth and M. Sander, Electron-Donating Phenolic and Electron-Accepting Quinone Moieties in Peat Dissolved Organic Matter: Quantities and Redox Transformations in the Context of Peat Biogeochemistry, *Environ. Sci. Technol.*, 2018, **52**, 5236–5245.
22 Y. Algurainy and D. F. Call, Cathodic precipitation of calcium carbonate and its impact on the electrosorption of sodium in flow-through capacitive deionization, *Desalination*, 2024, **586**, 117853.
23 W. Yu, C. Chu and B. Chen, Enhanced Microbial Ferrihydrite Reduction by Pyrogenic Carbon: Impact of Graphitic Structures, *Environ. Sci. Technol.*, 2022, **56**, 239–250.
24 Q. Abbas, M. Mirzaeian, A. A. Ogwu, M. Mazur and D. Gibson, Effect of physical activation/surface functional groups on wettability and electrochemical performance of carbon/activated carbon aerogels based electrode materials for electrochemical capacitors, *Int. J. Hydrogen Energy*, 2020, **45**, 13586–13595.
25 NIST X-ray Photoelectron Spectroscopy Database, **https://srdata.nist.gov/xps/SpectraIdentifier**, (accessed 18 March 2025).
26 Measurlabs, CHNOS analysis of organic materials | Measurlabs, **https://measurlabs.com/products/chnos-analysis/**, (accessed 10 April 2025).
27 Measurlabs, CHN(O)S Elemental Analysis | Measurlabs, **https://measurlabs.com/methods/chnos-elemental-analysis/**, (accessed 10 April 2025).
28 J. Schönherr, J. Buchheim, P. Scholz and P. Adelhelm, Boehm Titration Revisited (Part I): Practical Aspects for Achieving a High Precision in Quantifying Oxygen-Containing Surface Groups on Carbon Materials, *C*, 2018, **4**, 21.
29 R. B. Fidel, D. A. Laird and M. L. Thompson, Evaluation of Modified Boehm Titration Methods for Use with Biochars, *J. Environ. Qual.*, 2013, **42**, 1771–1778.
30 Kynol.de, **https://www.kynol.de/products.html**, (accessed 18 March 2025).
31 S. Wu, G. Fang, Y. Wang, Y. Zheng, C. Wang, F. Zhao, D. P. Jaisi and D. Zhou, Redox-Active Oxygen-Containing Functional Groups in Activated Carbon Facilitate Microbial Reduction of Ferrihydrite, *Environ. Sci. Technol.*, 2017, **51**, 9709–9717.
32 Analysis of Surface Area and Porosity in Biochar - Celignis Biomass Laboratory, **https://www.celignis.com/biochar-surface-area.php**, (accessed 18 March 2025).
33 P. Stelmachowski, J. Duch, D. Sebastián, M. J. Lázaro and A. Kotarba, Carbon-Based Composites as Electrocatalysts for Oxygen Evolution Reaction in Alkaline Media, *Materials*, 2021, **14**, 4984.
34 T. Mei, M. Gao, D. Liu, Y. Wang and Y. Huang, Enhanced electrocatalytic activity of carbon cloth by synergetic effect of plasma and acid treatment, *Plasma Sci. Technol.*, 2021, **23**, 025504.
35 C. Kim, P. Srimuk, J. Lee, S. Fleischmann, M. Aslan and V. Presser, Influence of pore structure and cell voltage of activated carbon cloth as a versatile electrode material for capacitive deionization, *Carbon*, 2017, **122**, 329–335.
36 Z. Hu and M. P. Srinivasan, Mesoporous high-surface-area activated carbon, *Microporous Mesoporous Mater.*, 2001, **43**, 267–275.
37 J. P. Chen and S. Wu, Acid/Base-Treated Activated Carbons: Characterization of Functional Groups and Metal Adsorptive Properties, *Langmuir*, 2004, **20**, 2233–2242.
38 E. Wolak and A. Orzechowska-Zięba, Change of the surface and structure of activated carbon as a result of HNO3 modification, *Adsorption*, 2024, **30**, 121–128.
39 Z. Li, J. Mao, W. Chu and W. Xu, Probing the Surface Reactivity of Pyrogenic Carbonaceous Material (PCM) through Synthesis of PCM-Like Conjugated Microporous Polymers, *Environ. Sci. Technol.*, 2019, **53**, 7673–7682.
40 Y. Zhang, X. Xu, L. Cao, Y. S. Ok and X. Cao, Characterization and quantification of electron donating capacity and its structure dependence in biochar derived from three waste biomasses, *Chemosphere*, 2018, **211**, 1073–1081.
41 C. L. Mangun, K. R. Benak, M. A. Daley and J. Economy, Oxidation of Activated Carbon Fibers: Effect on Pore Size, Surface Chemistry, and Adsorption Properties, *Chem. Mater.*, 1999, **11**, 3476–3483.
42 Carbon|XPS Periodic Table – US, **https://www.thermofisher.com/us/en/home/materials-science/learning-center/periodic-table/non-metal/carbon.html**, (accessed 18 March 2025).
43 Oxygen 1s for Organic Compounds, **https://www.xpsfitting.com/2013/08/oxygen-1s-for-organic-compounds.html**, (accessed 18 March 2025).
44 X. Zhang, J. Xia, J. Pu, C. Cai, G. W. Tyson, Z. Yuan and S. Hu, Biochar-Mediated Anaerobic Oxidation of Methane, *Environ. Sci. Technol.*, 2019, **53**, 6660–6668.
45 B. Singh, Y. Fang, B. C. C. Cowie and L. Thomsen, NEXAFS and XPS characterisation of carbon functional groups of fresh and aged biochars, *Org. Geochem.*, 2014, **77**, 1–10.
46 P. Zhang, J. Zhang, Z. Sun, C. He, B. Pan and B. Xing, The conductivity and redox properties of pyrolyzed carbon mediate methanogenesis in paddy soils with ethanol as substrate, *Sci. Total Environ.*, 2021, **795**, 148906.

47 S. Li, L. Shao, H. Zhang, P. He and F. Lü, Quantifying the contributions of surface area and redox-active moieties to electron exchange capacities of biochar, *J. Hazard. Mater.*, 2020, **394**, 122541.
48 B. Yi, F. Guo, Q. Wei, F. Huang, S. S. Senadheera, O. Mašek, A. K. Sarmah, J. Rinklebe and Y. S. Ok, Functionalized Biochar: Mechanisms of Oxygen-Containing Functional Groups in Water Pollutant Remediation, *ACS EST Water*, 2025, **5**(10), 5764–5784.
49 C. Passiu, A. Rossi, M. Weinert, W. Tysoe and N. D. Spencer, Probing the outermost layer of thin gold films by XPS and density functional theory, *Appl. Surf. Sci.*, 2020, **507**, 145084.
50 E. Kabir, K.-H. Kim and E. E. Kwon, Biochar as a tool for the improvement of soil and environment, *Front. Environ. Sci.*, 2023, **11**, 1324533.
51 J. Zhou, P. Yang, P. A. Kots, M. Cohen, Y. Chen, C. M. Quinn, M. D. de Mello, J. Anibal Boscoboinik, W. J. Shaw, S. Caratzoulas, W. Zheng and D. G. Vlachos, Tuning the reactivity of carbon surfaces with oxygen-containing functional groups, *Nat. Commun.*, 2023, **14**, 2293.
52 R. C. Prince, P. L. Dutton and M. R. Gunner, The aprotic electrochemistry of quinones, *Biochim. Biophys. Acta, Bioenerg.*, 2022, **1863**, 148558.
53 M. Sarewicz and A. Osyczka, Electronic Connection Between the Quinone and Cytochrome *c* Redox Pools and Its Role in Regulation of Mitochondrial Electron Transport and Redox Signaling, *Physiol. Rev.*, 2015, **95**, 219–243.
54 M. Ghorbani, E. Amirahmadi, R. W. Neugschwandtner, P. Konvalina, M. Kopecký, J. Moudrý, K. Perná and Y. T. Murindangabo, The Impact of Pyrolysis Temperature on Biochar Properties and Its Effects on Soil Hydrological Properties, *Sustainability*, 2022, **14**, 14722.
55 Y. Li, J. M. Kemper, G. Datuin, A. Akey, W. A. Mitch and R. G. Luthy, Reductive dehalogenation of disinfection byproducts by an activated carbon-based electrode system, *Water Res.*, 2016, **98**, 354–362.
56 I. Gerber, M. Oubenali, R. Bacsa, J. Durand, A. Gonçalves, M. F. R. Pereira, F. Jolibois, L. Perrin, R. Poteau and P. Serp, Theoretical and Experimental Studies on the Carbon-Nanotube Surface Oxidation by Nitric Acid: Interplay between Functionalization and Vacancy Enlargement, *Chem. – Eur. J.*, 2011, **17**, 11467–11477.
57 V. Gómez-Serrano, M. Acedo-Ramos, A. J. López-Peinado and C. Valenzuela-Calahorro, Oxidation of activated carbon by hydrogen peroxide. Study of surface functional groups by FT-i.r., *Fuel*, 1994, **73**, 387–395.
58 O. V. Bityukov, P. Y. Serdyuchenko, A. S. Kirillov, G. I. Nikishin, V. A. Vil' and A. O. Terent'ev, Advances in radical peroxidation with hydroperoxides, *Beilstein J. Org. Chem.*, 2024, **20**, 2959–3006.
59 G. Fang, C. Liu, J. Gao and D. Zhou, New Insights into the Mechanism of the Catalytic Decomposition of Hydrogen Peroxide by Activated Carbon: Implications for Degradation of Diethyl Phthalate, *Ind. Eng. Chem. Res.*, 2014, **53**, 19925–19933.
60 Z. Li, G. Song, X. Yang and Q. Song, Mechanism of $O_2$-promoted NO adsorption on activated carbon: an experimental and computational study, *Chem. Eng. J.*, 2024, **481**, 148391.
61 D. Ucar, Y. Zhang and I. Angelidaki, An Overview of Electron Acceptors in Microbial Fuel Cells, *Front. Microbiol.*, 2017, **8**, 643.
62 Hydrophilic and Hydrophobic|Research Starters|EBSCO Research, **https://www.ebsco.com**, (accessed 4 November 2025).
63 L. Yu, Y. Wang, Y. Yuan, J. Tang and S. Zhou, Biochar as Electron Acceptor for Microbial Extracellular Respiration, *Geomicrobiol. J.*, 2016, **33**, 530–536.
64 P. Liu, S. Sun, S. Huang, Y. Wu, X. Li, X. Wei and S. Wu, KOH Activation Mechanism in the Preparation of Brewer's Spent Grain-Based Activated Carbons, *Catalysts*, 2024, **14**, 814.
65 M. S. Hafizuddin, C. L. Lee, K. L. Chin, P. S. H'ng, P. S. Khoo and U. Rashid, Fabrication of Highly Microporous Structure Activated Carbon via Surface Modification with Sodium Hydroxide, *Polymers*, 2021, **13**, 3954.